Received: 11 July 2024 | Revised: 18 November 2024 | Accepted: 17 July 2025 | Published online: 12 August 2025

RESEARCH ARTICLE

Journal of Optics and Photonics Research
2025, Vol. 00(00) 1–9
DOI: 10.47852/bonviewJOPR52023823

BON VIEW PUBLISHING

Photocatalytic Properties Under Ultraviolet Light Irradiation of NiO–ZnO Nanocomposites Prepared by Sol–Gel Method

B. S. Satavekar[1], S. V. Anekar[1] and B. S. Shirke[2*]

[1]*Tatyasaheb Kore Institute of Engineering and Technology, Shivaji University, India*

[2]*Yashwantrao Chavan Warana Mahavidyalaya, Shivaji University, India*

Abstract: The NiO–ZnO metal oxide nanocomposites were prepared by the sol–gel method and possess a high degree of purity, as indicated by the X-ray diffraction patterns. The morphology and elemental results were studied using scanning electron microscopy and energy-dispersive X-ray spectrometer, respectively. The degradation of dyes, specifically crystal violet (CV), through photocatalysis has been investigated under ultraviolet light using NiO–ZnO mixed metal oxide nanocomposites with p-n type heterojunctions. The energy band gap of pure NiO–ZnO composites was calculated using the Tauc plot of absorption spectra, and it is found to be 2.95 eV. The optimal properties for all photocatalysts were a pH of 9, an irradiation time of 175 min, a catalyst amount of 100 mg, and a dye concentration of 10 mg/L. Under these optimum conditions, the prepared photocatalysts degraded the CV dye by 98.22% for NiO–ZnO. The p-n semiconductors type (NiO–ZnO) nanocomposites having the highest activity for CV degradation could be attributed to charge transfer processes inhibiting electron-hole pair recombination. As a result, semiconducting composite-based nanocatalysts with high photocatalytic activity, such as NiO–ZnO, show promise for future industrial applications in removing undesirable organic pollutants from the environment.

Keywords: photocatalytic, sol–gel, nanocomposite, semiconductors, XRD, BET (Brunauer–Emmett–Teller)

1. Introduction

All living things in this universe depend on clean, healthy water to survive. Overindustrialization has a negative impact on our freely available water resources [1]. Recently, issues related to water pollution have received much attention. Water pollution from dye-contaminated wastewater accounts for a significant portion of aqueous pollution. Several industries like food processing, textile dyeing, paints, papermaking, and cosmetics discharge dye-contaminated effluents into the environment, producing dye-contaminated wastewater. It is observed that, each year, about one million tons of dyes are made around the world. More than 15% of these dyes enter the environment as pollutants via industrial effluents [2].

According to multiple studies, the textile industry uses between 10 and 12% of dyes annually, including Eriochrome Black-T, Rhodamine B, Methylene Blue, Victoria blue, Thymol blue, Indigo Red, Caramine, and Rose Bengal [3–6]. Of these, about 20% are lost during the material's production and processing and wind up as wastewater. These dye-polluted effluents contain highly poisonous, nonbiodegradable colored dyes that have an adverse effect on living things [7].

Methyl violet 10 B, sometimes referred to as gentian violet or crystal violet (CV), is a triaryl methane dye that finds extensive application in several industries, including analytic chemistry, food processing, cosmetics, paper, leather, dyeing, and ballpoint pens. It is also possible to stain biological substances with CV. In biochemistry, CV has been used to measure cell viability because it binds to DNA. But in living tissue, this binding to DNA will cause replication mistakes, which could result in mutations and cancer. Toxicological studies have demonstrated that CV causes mutagenesis and carcinogenesis in animals. It is therefore regarded as a significant contaminant in wastewater [8].

Industrial wastewaters have been treated using a variety of techniques, including biological, chemical, food, dye processing, pulp and paper, textile waste, and pharmaceutical. Ultrafiltration, reverse osmosis, adsorption on activated carbon, chemical coagulation, and ion exchange on synthetic adsorbent resins are examples of traditional physical methods for eliminating color pollution [9].

Adsorption, nanofiltration, photooxidation, coagulation, reverse osmosis, and electrodialysis are a few of the removal methods that have been employed. Every approach has advantages and disadvantages of its own [10, 11]. Photocatalysis has many advantages, including environmental friendly, inexpensive, easy to operate, operate continuously under light sources, doesn't create

*Corresponding author: B. S. Shirke, Yashwantrao Chavan Warana Mahavidyalaya, Shivaji University, India. Email: bajiraoshirke@ycwm.ac.in

secondary waste, complete degradation, and reusable function at normal temperatures and atmospheric pressure. While many techniques have been employed, researchers have recently focused a great deal of attention on dye removal through a photocatalytic degradation process. Toxic dye pollution is transformed into harmless compounds using this environmentally friendly method. A cost-effective and highly efficient approach is transforming contaminated water into clean, fresh water. One of the most prevalent elements in our environment is solar light. The optimum way to employ photocatalysts in the process of photocatalysis, which degrades pollutants in water, is therefore outside.

The distinctive qualities of transition metal oxides (TMOs) such as their good chemical stability, environmental friendliness, high theoretical specific capacity at a reasonable cost, wide availability, and simple production process have garnered a lot of interest. The unique properties of transition metal oxides, or TMOs, such as their low cost of fabrication, environmental friendliness, high theoretical specific capacity, good chemical stability, and widespread availability, have sparked interest in TMOs for use as photocatalysts, in solar cells, gas sensors, electrode materials, and other applications [12].

Because of their important optical and electrical properties, which are very helpful in building multifunctional nanoscale optoelectronic and electronic devices, there has been an increased demand recently for the development of nanosized semiconductors. Using semiconductor metal oxide in photocatalysis has been a promising technique in recent years, and it is receiving more attention in the wastewater treatment area in an effort to fully mineralize pollutants in environmental systems.

Numerous semiconductor photocatalysts for eliminating dyes from wastewater are available in the literature. SnO_2, CeO_2, TiO_2, ZnO, WO_3, V_2O_5, or ZnS are examples of n-type semiconductors; on the other hand, NiO, CuO, Mn_3O_4, Co_3O_4, or Cu_2S are examples of p-type semiconductors [13–23]. However, because electron-hole pairs in a photocatalytic process regenerate quickly, the dye removal efficiency is not necessarily substantial. By doping with metals, these materials' photocatalytic capabilities are growing. The prospective applications of nanocomposite materials comprising two distinct TMOs in photocatalytic performance have led to a recent surge in interest. NiO–ZnO nanocomposites are more effective photocatalysts than individual NiO or ZnO particles. Their photocatalytic activity increases with the concentration of NiO. NiO–ZnO nanocomposites are effective at removing dyes like methylene blue and rhodamine B. They can also remove acid violet.

Separating the electrons and holes created by photon absorption increases the efficiency of photocatalysts. Heterojunctions between two semiconductors are one way to separate photoinduced electrons and holes. There are six different types of heterojunctions: surface, Schottky, Z-scheme, step-scheme, conventional, and p-n type. The focus of study these days is on p-n junction photocatalysts. By raising the quantum yields of photocatalytic reactions, effective electron and photon separation enhances advanced oxidation processes [24]. Heterojunction structures not only improve the effective charge transfer but also broaden the absorption of ultraviolet light in the photocatalytic system. Thus, photocatalytic and photoelectrochemical efficiency can be significantly enhanced under ultraviolet light illumination.

The literature review reveals that a number of techniques, such as sol–gel, microwave-assisted method, chemical vapor deposition, electrodeposition, spray pyrolysis, microemulsion, thermal decomposition of organic precursors, ultrasonic, and hydrothermal methods, have been developed for the synthesis of ZnO nanopowders. While the chemical method has gained popularity, most of these procedures are not used on a large basis [25].

Group II–VI semiconducting material with a high excitation energy is zinc oxide (ZnO). It is a broad band gap material with n-type semiconductivity with an energy of about 3.37 eV. Owing to its special qualities, it has been applied in a number of industries, such as photodetectors and photocatalysts, solar cells, varistors, optoelectronics, piezoelectric sensors, gas sensors, and light-emitting diodes [26–29]. Numerous morphological features, such as nanoparticles, nanorods, nanowires, and nanoflowers, can be easily shaped from zinc oxide (ZnO). In addition, it is nontoxic, easily prepared, and competitively priced [31]. Zinc oxide is polytypic, meaning it has several stable structural configurations. For instance, its hexagonal form is known as wurtzite, and its cubic structure is known as a zinc mix. Zinc oxide, an amphoteric oxide, has certain physical properties, such as its crystal structure and near insolubility in water and alcohol [30].

The green crystalline solid nickel oxide (NiO) possesses ferromagnetic characteristics. Above 523 K, it displays paramagnetic. It is a semiconductor material of the p-type with a broad band gap of roughly 3.6–4.0 eV in energy. The structure of NiO is face-centered cubic, or FCC. It can be used in a wide range of electronic and magnetic devices. These applications are improved when the particle size is controlled. NiO has emerged as an interesting study material because of its inexpensive cost and good ion storing characteristics [31].

NiO-ZnO nanocomposite p–n heterojunction semiconductors are gaining popularity due to their excellent electrical properties. They are widely used in electrochemical sensing, antibacterial applications, photocatalysts, gas sensing, and as a fuel cell electrodes. Additionally, they are employed magnetic recording devices. By doping ZnO with transition metals like Ni, this study improved and optimized its electrical, magnetic, and optical properties; the end product was the creation of novel materials that could find application in semiconductor systems. The p-n type (NiO–ZnO) nanocomposite has the maximum activity for dye degradation because of the charge transfer mechanisms that prevent electron-hole pair recombination [32]. This is most likely attributed to band gap energy variance.

In this work, the sol–gel synthesis of NiO–ZnO nanocomposites under UV light conditions was investigated for their enhanced catalytic oxidation of CV. Characterization techniques employed to assess the nanocomposites included X-ray diffraction (XRD), Fourier-transform infrared spectroscopy (FTIR), diffuse reflectance spectroscopy (DRS), transmission electron microscopy (TEM), Brunauer–Emmett–Teller (BET), thermogravimetric analysis (TGA), and UV-visible (UV-Vis) spectroscopy.

2. Materials and Procedures

2.1. Substances and agents

Analytical-grade chemicals were all utilized in the preparation process; no additional purification was necessary. The precursors were obtained from Sigma Aldrich and included nickel chloride hexahydrate ($NiCl_2$•$6H_2O$), zinc chloride hexahydrate ($ZnCl_2$•$6H_2O$), ammonia (NH_4OH), and ethylene glycol. Throughout the process, the solvent was deionized water. Aqueous solution was used to clean every piece of glassware, and deionized water was used to rinse it multiple times.

2.2. Preparation of NiO–ZnO nanocomposites

Using the sol–gel technique, ZnO-doped NiO nanocomposites were created with the formula $Ni_xZn_{1-x}O$ ($x = 0.1$). Following the proper ratios of (0.1 M) precursor solutions, the mixture was continuously heated to 80°C while being agitated. After letting the

liquid settle to ambient temperature, 0.1 M aqueous ammonia was gradually added dropwise until the mixture's pH reached approximately 10–11. Following pH adjustment, the mixture was stirred and allowed to settle for a full day. After removing the byproducts with deionized water, the resulting green precipitate was dried for 24 h at roughly 60°C. To neutralize the solution, it was repeatedly washed with double-distilled water. The solution was dried for 24 h at 100°C once it reached neutrality. The composite's dry precipitate was ground using an agate pestle and mortar, and it was then annealed for four hours at 400°C in a regulated muffle furnace. XRD analysis was used to track the composite sample's phase purity and degree of crystallinity.

2.3. Characterization of NiO–ZnO nanocomposite materials

On a Siemens D-500 diffractometer running at 45 kV and 100 mA, the powder materials' XRD was measured using Cu-Kα (λ = 1.5406 Å). At a scanning rate of 5°/min, the XRD pattern was recorded between angles of 10 and 80° (2θ). A Jasco UV-Vis-NIR spectrophotometer (model V-770) was used to record UV-Vis absorption spectra in the 200–800 nm wavelength range. The powder sample was studied using TEM on a JEOL JEM 2100 plus (Japan) apparatus. An SDT Q600 apparatus (TA Instruments, USA) was used to record the results of differential scanning calorimetry (DSC) and TGA. The sample was subjected to FTIR using an Agilent Technologies Cary 630 FTIR instrument. A Quanta Chrome Instruments v11.02 model was used to conduct BET experiments on the powder samples.

3. Results and Discussion

3.1. X-ray diffraction

XRD was used to characterize the nature and size of the particles. The pure NiO–ZnO nanocomposites' XRD patterns are displayed in Figure 1. The XRD pattern shows that there are no further impurity phases, indicating that Admina excellent NiO–ZnO nanocomposite material was synthesized.

The p-NiO cubic crystalline structure's (hkl) planes and 2θ values are determined to be 37.21° (111), 43.23° (200), and 62.82° (220), respectively (JCPDS no. 01-078-0423) [31]. The hexagonal crystalline structure of n-ZnO has the following diffraction peaks at 2θ values and (hkl) planes: 31.74° (100), 34.4° (002), 36.22° (101), 47.52° (102), 56.58° (110), 62.86° (103), 66.40° (200), 67.94° (112), and 69.10° (201) (JCPDS no. 01-079-2205) [26]. Using the following Scherrer equations, we estimated the average crystallite size (D) and strain (ε) present in the sample from the full width at half maximum (FWHM) of the XRD peaks in order to assess the impact of ZnO nanoparticles on the microstructural properties (such as size and strain) of NiO:

$$D = \frac{k\lambda}{\beta \cos\theta} \tag{1}$$

where θ is Bragg's diffraction angle, β = 1.54056 Å is the wavelength of Cu kα, β is the FWHM in radian intensity, D is the average crystallite size, ε is the lattice strain, and K is a constant, assumed to be 0.94.

It was found that the average D value of NiO–ZnO nanocomposites was 18 nm. For hexagonal ZnO, the lattice parameters computed from the XRD data are a = 4.68 Å, b = 3.43 Å, and c = 5.14 Å; for cubic NiO, they are a = 4.19 Å.

3.2. UV–Vis DRS spectral study

Using UV-Vis spectroscopy, the optical phenomena of the produced materials were examined. Optical absorption spectroscopy in the 200–800 nm wavelength range is displayed in Figure 2(a). The Tauc formula, which is as follows, serves as the foundation for the DRS study of the absorbing substance.

$$\alpha h\upsilon = B(h\upsilon - Eg)^n \tag{2}$$

where α (2.303 A/d) is the coefficient of absorption, A is the absorbance, d is the optical path length, B is the proportionality constant, Eg is the band gap energy, hν is the energy of the photon, and n is a constant that is found to be ½ for direct

Figure 1
XRD patterns of (a) pure NiO, (b) pure ZnO, and (c) NiO–ZnO nanocomposites

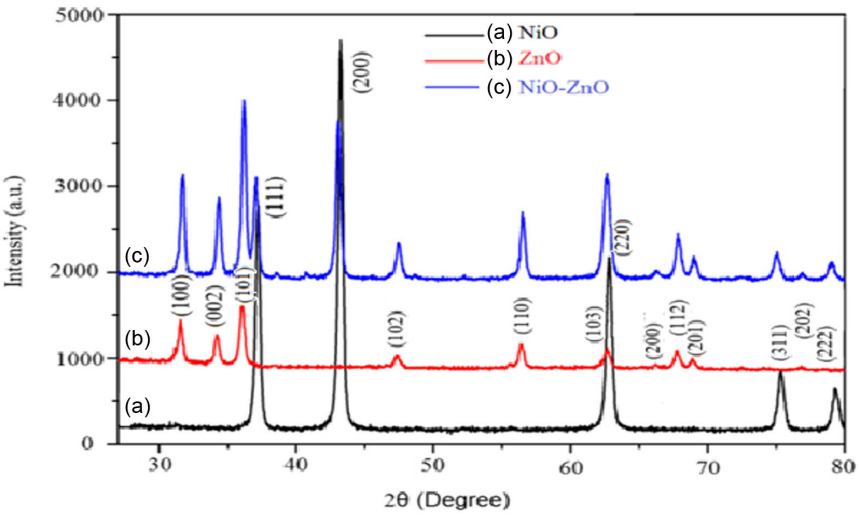

Figure 2
(a) UV–visible absorption spectrum of the NiO–ZnO nanocomposite and (b) Tauc plot of the NiO–ZnO nanocomposite

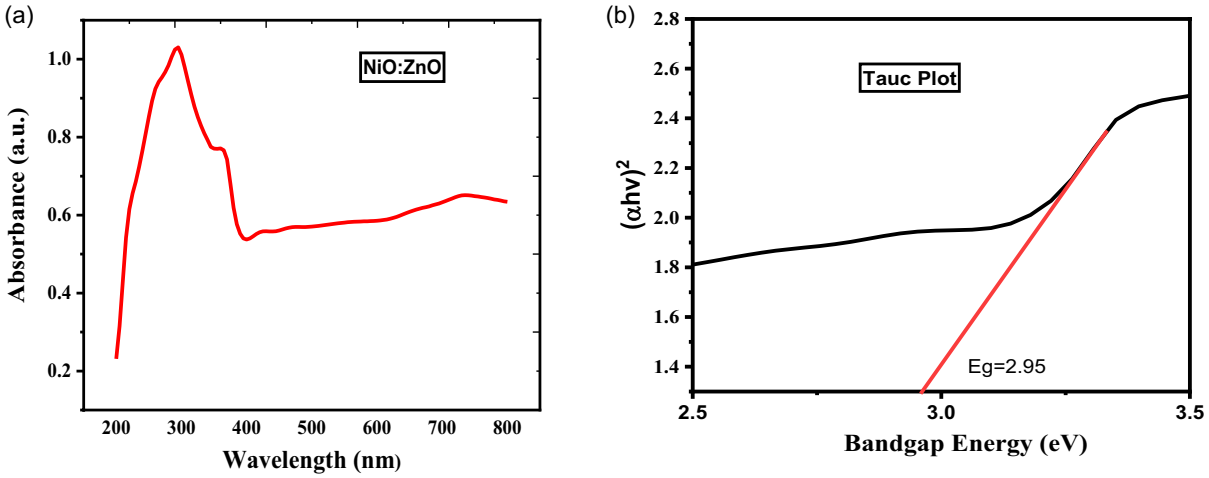

allowed transitions and 2 for indirect allowed transitions. As demonstrated in Figure 2(b), the optical band gaps of the produced samples were determined by the use of a Tauc plot, which involved graphing $(\alpha h\upsilon)^2$ vs $(h\upsilon)$, which is 2.95 eV.

3.3. Compositional analysis (EDS)

The energy-dispersive X-ray spectrometer (EDS) data resolution was noted in the binding energy region of 0–20 keV as shown in Figure 3. The spectrum's peak indicates that Ni, Zn, and O are present. Ni, Zn, and O have atomic percentages of 35.01, 42.12, and 22.87%, in that order. The current ratio of Ni, Zn, and O indicates that nonstoichiometric NiO–ZnO forms, which makes them effective photocatalysts for use in photocatalytic processes.

3.4. Transmission electron microscopy (TEM)

NiO–ZnO was subjected to TEM examination in order to learn more about the internal microstructure and crystallographic characteristics of the nonmaterial; the resulting TEM patterns are displayed in Figure 4. The aggregation of the growing ZnO and NiO particles is the reason for the nanocomposite's greater range of particle sizes.

The TEM picture reveals the presence of cubic and hexagonal structures. Mesoporous structure development is indicated by the interconnectivity of nanoparticles. The TEM picture of the NiO–ZnO nanocomposites shows that the particles are roughly 20 nm in size.

3.5. Fourier-transform infrared spectroscopy (FTIR)

Utilizing FTIR, the distinctive functional groups present in the NiO–ZnO nanocomposites were identified. Figure 5 displays the synthesized nanocomposites' FTIR spectrum. The produced nanocomposites' spectra showed the presence of absorption bands in the 400–4000 cm^{-1} range. At about 3367 cm^{-1}, a large absorption peak due to O-H stretching was seen. The minor peak at 913 cm^{-1} is attributed to C–H stretching, while the peaks at 1560 cm^{-1} and 1395 cm^{-1} are assigned to the symmetric and asymmetric C=O stretching vibration modes. The metal-oxygen bond vibrations are correlated with the drop at 638 cm^{-1}. The stretching mode of the Zn–O bond is responsible for the signal that was detected at 430 cm^{-1}. A novel vibration mode at 513 cm^{-1}, corresponding to the Ni–O stretching bond, is visible in the spectra of ZnO and ZnO

Figure 3
EDS image of the NiO–ZnO nanocomposite

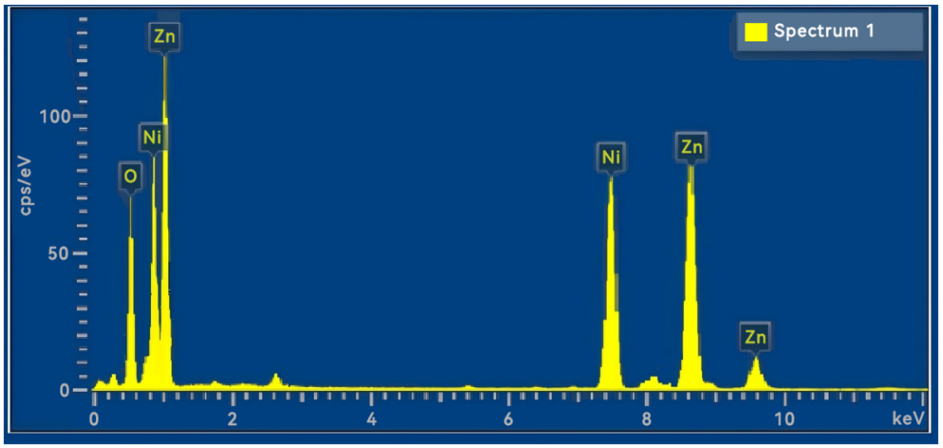

Figure 4
TEM image of the NiO–ZnO nanocomposite

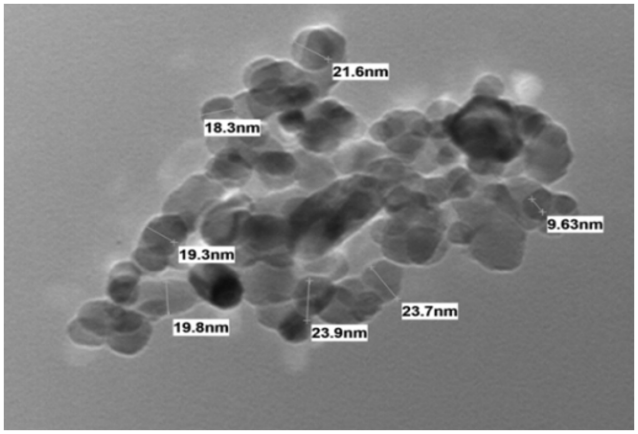

Figure 5
FTIR image of the NiO–ZnO nanocomposite

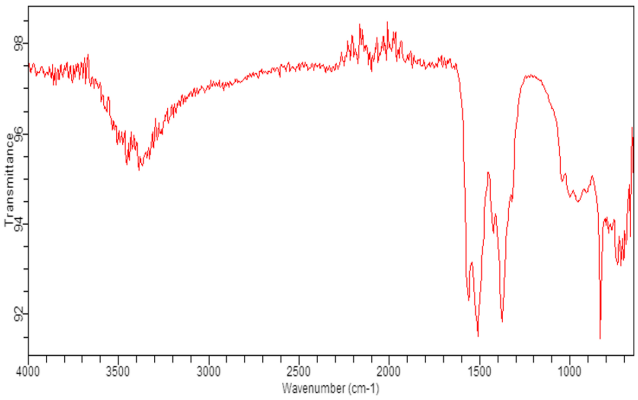

doped with NiO at various molar ratios of NiO–ZnO nanocomposites, indicating that NiO was successfully doped into ZnO.

3.6. Thermal analysis

As illustrated in Figure 6, the thermal behavior of the produced NiO–ZnO nanocomposites was examined using TGA and DSC analysis at 20–800°C at a heating rate of 10°C/min in a nitrogen atmosphere. Two stages of decomposition were detected by TGA of the sample. Water molecules and evaporation were seen in the first stage, which was followed by dehydration from below 21°C to 180°C, reaching a maximum at 60°C. Alongside this decline, there was a mass loss of roughly 0.08616 mg, or 0.7818%. Two molecules of carbon dioxide and two molecules of nitrogen dioxide underwent thermal degradation in the second stage between 180°C and 295°C. The mass loss that accompanied it was estimated to be 4.198%, or 0.4626 mg. The third stage was exothermic, with the loss of two water molecules between 295°C and 500°C, with a maximum at 400°C, converting hydroxides to oxides. A mass reduction of about 0.6757%, or about 0.07447 mg, was also observed with it. At temperatures over 500°C to 800°C, there was no discernible shift in weight. The absence of alteration indicates that ZnO nanoparticles are present. Since there was no change in weight loss or thermal impacts over 800°C, the TG-DSC results supported the crystalline nature of the NiO–ZnO nanocomposites.

3.7. Brunauer–Emmett–Teller (BET) surface area analysis

To ascertain the nanocomposites' precise surface area, surface area analysis was carried out. Figure 7 displays the type IV, N2 sorption isotherms of the produced nanocomposites, which demonstrate the presence of slit-like mesoporous (2–50 nm) nanoparticles created by aggregation. The findings of the BET study showed that the pore size was 1.807 nm, the pore volume was 0.049 cc/g, and the surface area was 31.485 m^2/g. The results clearly show that there is an inverse relationship between surface area and particle size in nanocomposites. The distribution of pore sizes in the samples confirmed the formation of mesoporous material. A greater surface area can result in enhanced photocatalytic activity because there are more active surface sites available for improved dye molecule adsorption.

3.8. The photocatalytic degradation factors

3.8.1. pH's impact

The pH of the solution is one of the key variables in photocatalytic processes. It significantly affects the photocatalyst's surface charge. As seen in Figure 8, the impact of solution pH on the rate of photocatalytic degradation in the presence of NiO–ZnO was examined throughout a range of pH values from 3 to 11. According to the experimental findings, as the pH rose from 3 to 11, there was a noticeable rise in the rate of photocatalytic degradation of CV. The process of dye degradation becomes constant above pH 9. The large concentration of protons in acidic solutions ($pH < 6$) slows down the dye's photodegradation, leading to a reduced degradation efficiency. A change in the shape of the material was observed by varying the pH. It is found that as pH increases, the luminescence intensity in the UV region increases. The significant adsorption and high degradation rate are caused by basic pH electrostatic interactions between the catalyst surfaces and CV cations. The best pH was determined to be nine, and at that pH, the catalyst and NiO–ZnO had a dye removal rate of 97.71%.

3.8.2. Impact of contact time

Another factor influencing the photocatalytic efficiency of NiO–ZnO, a nanocatalyst, in the elimination of CV dye is the irradiation time. The study examined the experiment at an optimal pH of 9, maintaining constant other experimental parameters but varying the irradiation time from 30 to 180 min. The degradation efficiency versus irradiation time is illustrated in Figure 9. Up to 150 min of increasing irradiation, the produced photocatalysts for CV showed an increase in degradation efficiency; after that, the value stayed constant. This catalyst enhances the photodegradation of CV compared to ZnO and higher dopant concentrations. The incorporation of NiO ions decreases the optical band gap of ZnO samples, which contributes to the development of O^{2-}. For all the samples, the ideal irradiation duration was 180 min, and the NiO–ZnO catalysts had a dye removal efficiency of 98.22%.

3.8.3. Impact of dye concentration

An experiment was carried out at an optimal pH of 9 and irradiation length of 180 min by varying the CV concentration from 5 to 20 mg/L in order to ascertain the effect of dye concentration on the degradation effectiveness of the manufactured photocatalyst. Figure 10 displays the CV deterioration efficiency findings that were obtained. The graph

Figure 6
TGA/DSC image of the NiO–ZnO nanocomposite

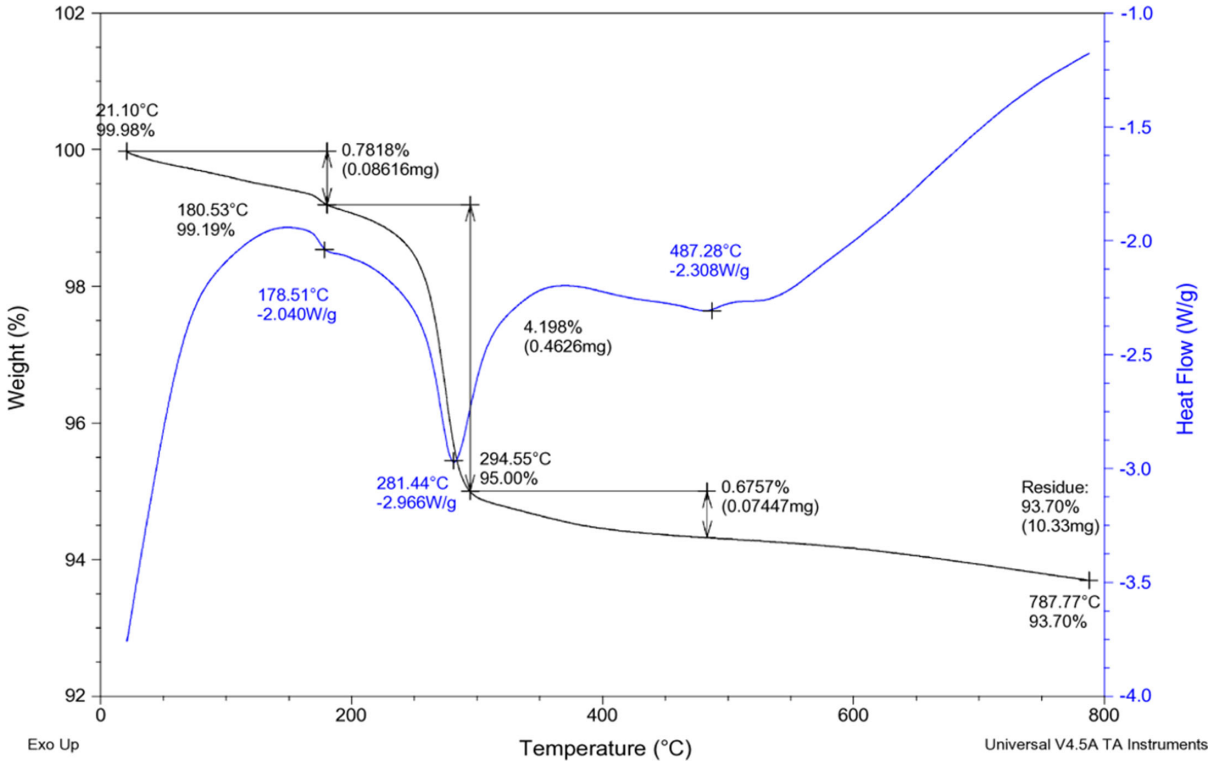

unequivocally demonstrates that the relationship between the dye concentration and the produced photocatalyst's degradation efficiency is inverse. Under UV radiation, the degradation efficiency falls as dye concentration rises. Since OH radical generation is constant for a given amount of catalyst, the percentage of dye degradation drastically falls over a certain concentration due to inadequate OH radicals.

The production of radicals by the photocatalyst and the radicals' interactions with dye molecules determine the pace of degradation. Since the dye ions shield the photocatalyst's active sites, the generation of hydroxyl radicals (.OH) at the catalyst's surface is decreased at high dye concentrations. Moreover, ultraviolet radiation can be significantly absorbed by dye molecules at high dye concentrations, lowering the radiation level. Consequently, for all catalysts, the removal of CV was more effective at low concentrations, or 10 mg/L, with a removal efficiency of 92.44% for NiO–ZnO. For our additional research, we employed a concentration of CV of 10 mg/L. We have investigated how the dye deteriorates in relation to its concentration. Figure 10 demonstrates unequivocally that less degradation happened at higher doses. This results from an increase in dye concentration; more dye is absorbed by the catalyst

Figure 7
BET image of the NiO–ZnO nanocomposite

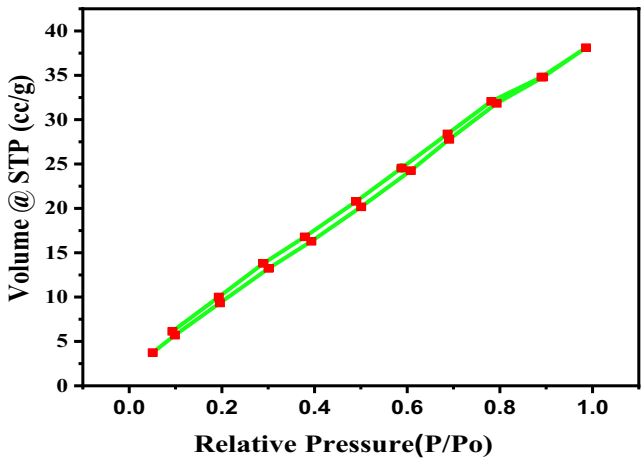

Figure 8
Effect of pH on the degradation of CV dye

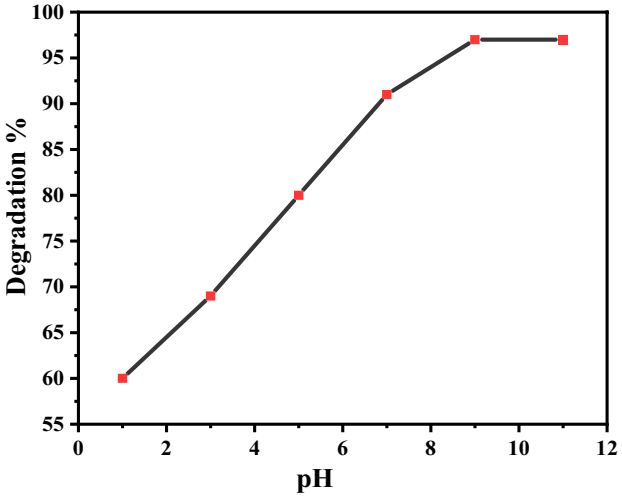

Figure 9
Effect of contact time on the degradation of CV dye

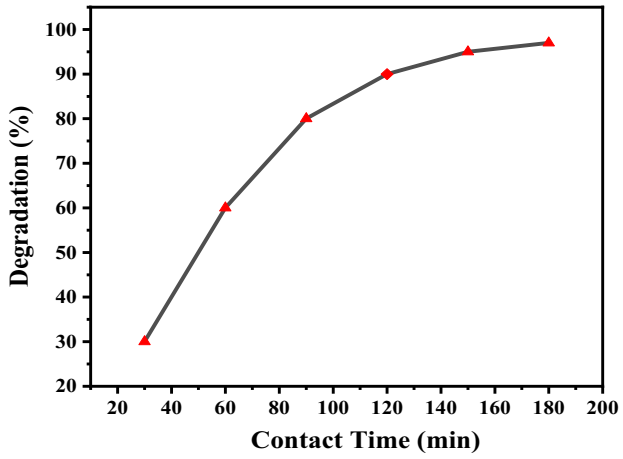

Figure 10
Effect of dye concentration on degradation of CV dye

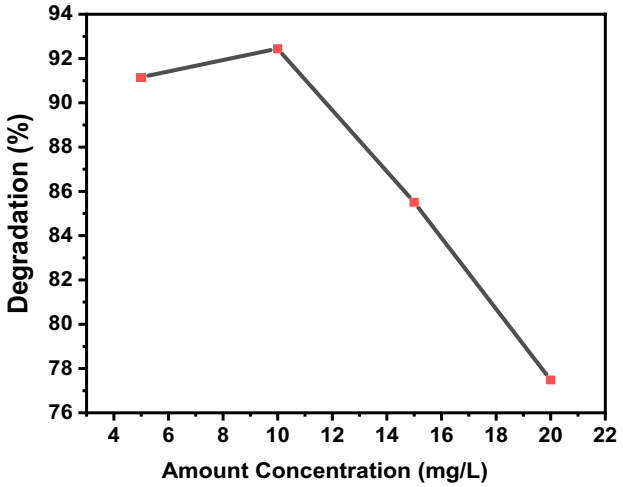

particles. UV light cannot therefore reach the catalytic surface. Light moves closer together at higher concentrations.

3.8.4. Impact of the catalyst

By changing the amount of dye solution from 50 to 200 mg, the photocatalyst's impact on the dye's percentage degradation was investigated, as illustrated in Figure 11. The dye degradation increased to a point where a decrease in the decolorization rate was noticed after the catalyst concentration was raised to 100 mg. This is due to the fact that the number of active sites needed for photocatalytic dye decolorization rises with catalyst concentration. Additionally, after adding 100 mg of catalyst to the dye solution, the suspension becomes more turbid and experiences a reduction in sunlight/UV penetration, which slows down the photodecolorization process. Based on the experimental findings, 100 mg of photocatalyst was determined to be the ideal amount. For the NiO–ZnO nanocomposite, the dye removal was 92.10% at the ideal dosage. Lastly, the ideal parameters for a photocatalytic degradation experiment were pH 9, 10 mg/L CV solution, 100 mg catalyst, and 175 min irradiation period for the NiO–ZnO photocatalysts.

Figure 11
Effect of catalyst on the degradation of CV dye

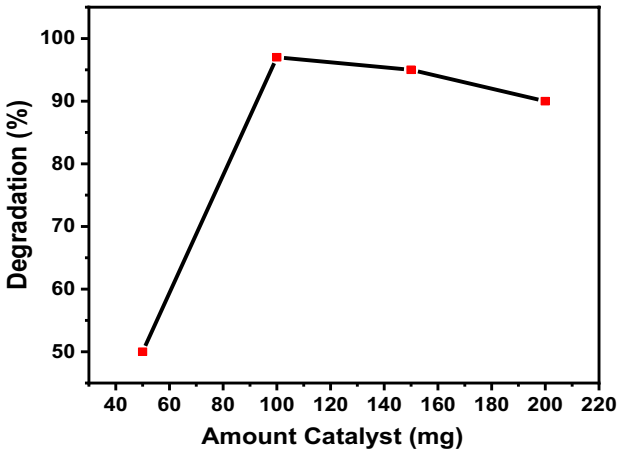

4. Conclusion

In conclusion, the sol–gel technique was utilized to successfully create NiO–ZnO nanocomposites with ethylene glycol acting as a solvent. Under UV light irradiation, this nanocatalyst was employed for the photocatalytic elimination of CV dye. The XRD patterns show that the metal oxides produced using the previously described process are highly pure. Scanning electron microscopy and EDS were used to analyze the morphological and elemental data, respectively. These materials have the potential to be effective photocatalysts, as demonstrated by the experimental results of CV dye photodegradation. The produced nanocomposite demonstrated excellent photocatalytic activity toward the degradation of CV, according to the results.

Acknowledgment

The laboratory facilities were provided by the Tatyasaheb Kore Institute of Engineering and Technology and the Institute of Yashwantrao Chavan Warana Mahavidyalaya, Waranagar, to which the authors are very thankful.

Ethical Statement

This study does not contain any studies with human or animal subjects performed by any of the authors.

Conflicts of Interest

The authors declare that they have no conflicts of interest to this work.

Data Availability Statement

Data sharing is not applicable to this article as no new data were created or analyzed in this study.

Author Contribution Statement

B. S. Satavekar: Conceptualization, Methodology, Software, Validation, Formal analysis, Investigation, Resources, Data curation, Writing – original draft, Writing – review & editing, Visualization. **S. V. Anekar:** Writing – review & editing, Project

administration. **B. S. Shirke:** Conceptualization, Methodology, Software, Validation, Formal analysis, Investigation, Resources, Data curation, Writing – original draft, Writing – review & editing, Supervision, Project administration.

References

[1] Yousaf, S., Zulfiqar, S., Din, M. I., Agboola, P. O., AlyAboud, M. F., Warsi, M. F., & Shakir, I. (2021). Solar light irradiated photocatalytic activity of ZnO-NiO/rGO nanocatalyst. *Journal of Materials Research and Technology*, *12*, 999–1009. https://doi.org/10.1016/j.jmrt.2021.03.012

[2] Saeed, M., Muneer, M., Haq, A. U., & Akram, N. (2022). Photocatalysis: An effective tool for photodegradation of dyes – a review. *Environmental Science and Pollution Research*, *29*(1), 293–311. https://doi.org/10.1007/s11356-021-16389-7

[3] George, A., Raj, D. M. A., Venci, X., Raj, A. D., Irudayaraj, A. A., Josephine, R. L., …, & Kaviyarasu, K. (2022). Photocatalytic effect of the degradation of methylene blue (MB) dye on CuO nanoparticle flower-like 3D nanostructures under visible light irradiation for environmental application. *Environmental Research*, *203*, 111880. https://doi.org/10.1016/j.envres.2021.111880

[4] Mai, F. D., Lu, C. S., Wu, C. W., Huang, C. H., Chen, J. Y., & Chen, C. C. (2008). Mechanisms of photocatalytic degradation of Victoria Blue R using nano-TiO_2. *Separation and Purification Technology*, *62*(2), 423–436. https://doi.org/10.1016/j.seppur.2008.02.006

[5] Kansal, S. K., Sood, S., Umar, A., & Mehta, S. K. (2013). Photocatalytic degradation of Eriochrome Black T dye using well-crystalline anatase TiO_2 nanoparticles. *Journal of Alloys and Compounds*, *581*, 392–397. https://doi.org/10.1016/j.jallcom.2013.07.069

[6] Goyal, S., & Patidar, D. (2022). Photocatalytic degradation of indigo caramine from an aqueous solution by TiO_2 nanoparticles under UV irradiation. *Journal of Advanced Scientific Research*, *13*(2), 183–189. https://doi.org/10.55218/JASR.202200000

[7] Rafiq, A., Ikram, M., Ali, S., Niaz, F., Khan, M., Khan, Q., & Maqbool, M. (2021). Photocatalytic degradation of dyes using semiconductor photocatalysts to clean industrial water pollution. *Journal of Industrial and Engineering Chemistry*, *97*, 111–128. https://doi.org/10.1016/j.jiec.2021.02.017

[8] Thattil, P. P., & Leema Rose, A. (2020). Enhanced removal of crystal violet dye using zinc oxide nanorods and air oxidation under sunlight radiation. *Rasayan Journal of Chemistry*, *13*(2), 1166–1173. https://doi.org/10.31788/RJC.2020.1325558

[9] Weldekirstos, H. D., Habtewold, B., & Kabtamu, D. M. (2022). Surfactant-assisted synthesis of NiO-ZnO and NiO-CuO nanocomposites for enhanced photocatalytic degradation of methylene blue under UV light irradiation. *Frontiers in Materials*, *9*, 832439. https://doi.org/10.3389/fmats.2022.832439

[10] Muhambihai, P., Rama, V., & Subramaniam, P. (2020). Photocatalytic degradation of aniline blue, brilliant green and direct red 80 using NiO/CuO, CuO/ZnO and ZnO/NiO nanocomposites. *Environmental Nanotechnology, Monitoring & Management*, *14*, 100360. https://doi.org/10.1016/j.enmm.2020.100360

[11] Isherwood, P. J. M., & Walls, J. M. (2014). Cupric oxide-based p-type transparent conductors. *Energy Procedia: Advanced Materials and Characterization Techniques for Solar Cells II*, *60*, 129–134.

[12] Hashem, M., Saion, E., Al-Hada, N. M., Kamari, H. M., Shaari, A. H., Talib, Z. A., …, & Kamarudeen, M. A. (2016). Fabrication and characterization of semiconductor nickel oxide (NiO) nanoparticles manufactured using a facile thermal treatment. *Results in Physics*, *6*, 1024–1030. https://doi.org/10.1016/j.rinp.2016.11.031

[13] Kabure, A. A., Mane, S. R., & Shirke B. S. (2020). The LPG gas sensing performance of CeO_2-CuO nanocomposite film synthesized by microwave assisted sol-gel method. *International Journal of Recent Scientific Research*, *11*(5), 38560–38567. https://doi.org/10.24327/ijrsr.2020.1105.5335

[14] Ichiyanagi, Y., Yamada, T., Kanazawa, Y., &Uehashi, T. (2006). Magnetic properties of Mn3O4 nanoparticles. In *Low Temperature Physics: 24th International Conference on Low Temperature Physics*, *850*(1), 1155–1156. https://doi.org/10.1063/1.2355113

[15] Makhlouf, S. A., Bakr, Z. H., Aly, K. I., & Moustafa, M. S. (2013). Structural, electrical and optical properties of Co_3O_4 nanoparticles. *Superlattices and Microstructures*, *64*, 107–117. https://doi.org/10.1016/j.spmi.2013.09.023

[16] Bhosale, T. T., Kuldeep, A. R., Pawar, S. J., Shirke, B. S., & Garadkar, K. M. (2019). Photocatalytic degradation of methyl orange by Eu doped SnO_2 nanoparticles. *Journal of Materials Science: Materials in Electronics*, *30*(20), 18927–18935. https://doi.org/10.1007/s10854-019-02249-1

[17] Liu, X., Zhai, H., Wang, P., Zhang, Q., Wang, Z., Liu, Y., …, & Zhang, X. (2019). Synthesis of a WO_3 photocatalyst with high photocatalytic activity and stability using synergetic internal Fe^{3+} doping and superficial Pt loading for ethylene degradation under visible-light irradiation. *Catalysis Science & Technology*, *9*, 652–658. https://doi.org/10.1039/C8CY02375A

[18] Shirke, B. S., Korake, P. V., Hankare, P. P., Bamane, S. R., & Garadkar, K. M. (2011). Synthesis and characterization of pure anatase TiO_2 nanoparticles. *Journal of Materials Science: Materials in Electronics*, *22*(7), 821–824. https://doi.org/10.1007/s10854-010-0218-4

[19] Sun, Y., Zhang, W., Li, Q., Liu, H., & Wang, X. (2023). Preparations and applications of zinc oxide based photocatalytic materials. *Advanced Sensor and Energy Materials*, *3*(2), 100069. https://doi.org/10.1016/j.asems.2023.100069

[20] Yu, Z. Y., Zhao, J. N., Yang, F., Tang, X. F., Wu, Y. F., Ma, C. F., …, & Meng, Q. W. (2020). Rose Bengal as photocatalyst: Visible light-mediated Friedel-Crafts alkylation of indoles with nitroalkenes in water. *RSC Advances*, *10*(8), 4825–4831. https://doi.org/10.1039/c9ra09227g

[21] Devarahosahalli Veeranna, K., Theeta Lakshamaiah, M., & Thimmasandra Narayan, R. (2014). Photocatalytic degradation of indigo carmine dye using calcium oxide. *International Journal of Photochemistry*, *2014*, 530570. https://doi.org/10.1155/2014/530570

[22] Saeed, M., Albalawi, K., Khan, I., Akram, N., Abd El-Rahim, I. H. A., Alhag, S. K., …, & Faiza. (2023). Synthesis of p-n NiO-ZnO heterojunction for photodegradation of crystal violet dye. *Alexandria Engineering Journal*, *65*, 561–574. https://doi.org/10.1016/j.aej.2022.09.048

[23] Mancuso, A., Blangetti, N., Sacco, O., Freyria, F. S., Bonelli, B., …, & Vaiano, V. (2023). Photocatalytic degradation of crystal violet dye under visible light by Fe-doped TiO_2

prepared by reverse-micelle sol–gel method. *Nanomaterials*, *13*(2), 270. https://doi.org/10.3390/nano13020270

[24] Hussein, I. F., Nusseif, A. D., & Majeed, A. M. A. (2020). Analytical study of ZnO-NiO nanocomposite of antibacterial activities. *Plant Archives*, *20*(1), 2747–2750.

[25] Chen, F., Ma, T. Y., Zhang, T. R., Zhang, Y. H., & Huang, H. W. (2021). Atomic-level charge separation strategies in semiconductor-based photocatalysts. *Advanced Materials*, *33*(10), 2005256. https://doi.org/10.1002/adma.202005256

[26] Talam, S., Karumuri, S. R., & Gunnam, N. (2012). Synthesis, characterization, and spectroscopic properties of ZnO nanoparticles. *International Scholarly Research Notices*, *2012*(1), 372505. https://doi.org/10.5402/2012/372505

[27] Kataria, S., Bala, S., Chand, S., Mahendia, S., Sinha, O. P., & Kumar, S. (2019). Synthesis and characterization of zinc oxide (ZnO) nanostructures. In *Proceedings of the National Conference on Recent Advances in Condensed Matter Physics*, *2093*(1), 020031. https://doi.org/10.1063/1.5097100

[28] Khan, J., Ilyas, S., Akram, B., Ahmad, K., Hafeez, M., Siddiq, M., . . . , & Ashraf, M. A. (2018). Zno-NiO coated multi walled carbon nanotubes for textile dyes degradation. *Arabian Journal of Chemistry*, *11*(6), 880–896. https://doi.org/10.1016/j.arabjc.2017.12.020

[29] Bonomo, M. (2018). Synthesis and characterization of NiO nanostructures: A review. *Journal of Nanoparticle Research*, *20*(8), 222. https://doi.org/10.1007/s11051-018-4327-y

[30] Rahdar, A., Aliahmad, M., & Azizib, Y. (2015). NiO nanoparticles: Synthesis and characterization. *Journal of Nanostructures*, *5*(2), 145–151. https://doi.org/10.7508/jns.2015.02.009

[31] Shamim, A., Ahmad, Z., Mahmood, S., Ali, U., Mahmood, T., & Nizami, Z. A. (2019). Synthesis of nickel nanoparticles by sol-gel method and their characterization. *Open Journal of Chemistry*, *2*(1), 16–20. https://doi.org/10.30538/psrp-ojc2019.0009

[32] Sundararajan, M., Sailaja, V., Kennedy, L. J., & Vijaya, J. J. (2017). Photocatalytic degradation of rhodamine B under visible light using nanostructured zinc doped cobalt ferrite kinetics and mechanism. *Ceramics International*, *43*(1), 540–548. https://doi.org/10.1016/j.ceramint.2016.09.191

How to Cite: Satavekar, B. S., Anekar, S. V., & Shirke, B. S. (2025). Photocatalytic Properties Under Ultraviolet Light Irradiation of NiO–ZnO Nanocomposites Prepared by Sol–Gel Method. *Journal of Optics and Photonics Research*. https://doi.org/10.47852/bonviewJOPR52023823